Phosphorene in ultrafast laser field

Fatemeh Nematollahi, Vadym Apalkov, and Mark I. Stockman

Phys. Rev. B **97**, 035407 — Published 5 January 2018

DOI: 10.1103/PhysRevB.97.035407

Phosphorene in ultrafast laser field

Fatemeh Nematollahi, Vadym Apalkov, and Mark I. Stockman
Center for Nano-Optics (CeNO) and Department of Physics and Astronomy, Georgia State University, Atlanta, Georgia 30303, USA
(Dated: November 7, 2017)

We study numerically interaction of phosphorene monolayer with a strong femtosecond-long optical pulse. For such a short pulse, the electron dynamics is coherent and can be described by the time-dependent Schrödinger equation. Strong optical field of the pulse causes redistribution of electrons between the conduction and valence bands. Such interband dynamics is highly irreversible, i.e., the conduction band population after the pulse is large and comparable to the maximum conduction band during the pulse. The conduction band population distribution in the reciprocal space shows high contrast hot spots, which are due to large interband coupling at the Γ point. The optical pulse also causes the net charge transfer through the phosphorene monolayer. The direction of the transfer is the same as the direction of the field maximum.

I. INTRODUCTION

Two dimensional materials have attracted much attention after remarkable topological, transport, and optical properties of graphene have been discovered both theoretically and experimentally[1–4]. Graphene has the honeycomb crystal structure with unique relativistic energy dispersion and chiral electron states. It is a semimetal with zero bandgap. For other 2D materials, such as silicene or germanene, which have crystal structure that is similar to graphene, a finite but small bandgap is opened due to relatively large spin-orbit interaction. Such bandgap can be controlled by an external electric field. In this relation, recently experimentally realized monolayer black phosphorus, phosphorene, has attracted much attention because of its relatively large bandgap, ~ 2 eV, which opens potential applications of phosphorene in optoelectronics and nanoelectronics[5–10].

In relation to potential applications of 2D materials, it is very important to understand how these materials respond to applied external electric field, especially to a strong electric field, which is comparable to internal fields in solids, ~ 1 V/Å. Such strong electric fields can modify both transport and optical properties of the materials and can be also used to control and probe them. Interaction of strong fields with solids has been the subject of intensive experimental and theoretical research[11–27]. Interest in this field has grown tremendously due to availability of ultrashort femtosecond-long pulses with strong fields, ~ 1 V/Å[16,20,28]. Such high fields can strongly modify properties of a solid within an optical cycle, resulting, for example, in metallization of dielectric at a femtosecond time scale[25–27]. Such metallization is detected as a finite charge transfer through a dielectric material during an ultrashort pulse[25,29]. Although the transport properties of the dielectric material are strongly modified during the pulse, the electron dynamics is highly reversible during the pulse, i.e., the electron system returns to its initial state after the pulse.

Interaction of graphene and graphene-like materials with strong and ultra-short pulses has been extensively studied theoretically[30–33]. It has been shown that the strong-field interactions of graphene-like materials are highly non-adiabatic and irreversible causing significant electron transfer from the valence band, which results in high population of the conduction band. Unique features of ultrafast electron dynamics in graphene-like materials are determined by specific properties of interband dipole coupling, which has singularities at the Dirac points. Such singularities result in the formation of highly localized hot spots in electron population distribution in the reciprocal space. The number of such hot spots is proportional to the field amplitude.

Here we study the strong-field interactions in another 2D material, phosphorene, which, in contrast to graphene-like materials, is characterized by a large bandgap, ≈ 2 eV. We show below that, although the phosphorene monolayer has relatively large bandgap, the electron dynamics in this material is highly irreversible, which is similar to graphene. The ultrafast electron dynamics in phosphorene is also characterized by a relatively large charge transfer through the system during the pulse.

II. MODEL AND MAIN EQUATIONS

We assume that an ultrashort optical pulse is incident normally on a phosphorene monolayer and has the following profile

$$F(t) = F_0 e^{-u^2}(1-2u^2), \tag{1}$$

where F_0 is the amplitude of the pulse, $u = t/\tau$, and τ is the pulse's duration. The experimentally realized profile of the ultrastrong optical pulse can be found in Ref.[26]. For the shape of the pulse given by Eq. (1), the area under the pulse is always zero, $\int_{-\infty}^{+\infty} \mathrm{F}(t)dt = 0$. Below we assume that $\tau = 1$ fs, which corresponds to the carrier frequency of $\omega \approx 1.5$ eV/$\hbar$. For such ultrashort pulse, the duration of which is less than the characteristic electron scattering time $\sim 10 - 100$ fs, the electron dynamics during the pulse is coherent and can be described by the time-dependent Schrödinger equation. The corresponding time-dependent electron Hamiltonian has the

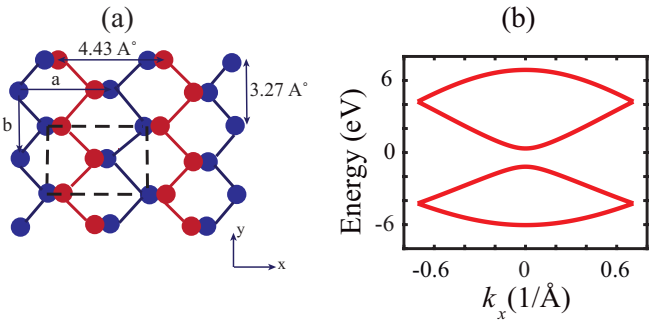

FIG. 1: (a) Lattice structure of 2D phosphorene. The red and blue dots represent phosphorous atoms in the upper and lower layers, respectively. The dashed lines show the primitive unit cell, which contains four atoms. The primitive vectors a and b are also shown. (b) Band structure of phosphorene obtained within the tight-binding model. Energy spectrum is shown as a function of k_x at $k_y = 0$.

following form

$$\mathcal{H} = \mathcal{H}_0 + e\mathbf{F}(t)\mathbf{r}, \tag{2}$$

where H_0 is the field-free electron Hamiltonian, $\mathbf{F}(t) = [F(t)cos(\theta), F(t)sin(\theta)]$, and $\mathbf{r} = (\mathbf{x}, \mathbf{y})$ is a two dimensional vector. Below we consider a linearly x-polarized pulse, i.e., $\theta = 0$.

We describe the free-electron system by the tight-binding Hamiltonian. The lattice structure of phosphorene is shown in Fig. 1, where the unit cell is marked by dashed lines. The unit cell contains four atoms. Such structure results in four-band tight binding Hamiltonian of the following form[10]

$$\mathcal{H}_0 = \begin{pmatrix} 0 & A_k & B_k & C_k \\ A_k^* & 0 & D_k & B_k \\ B_k^* & D_k^* & 0 & A_k \\ C_k^* & B_k^* & A_k^* & 0 \end{pmatrix}, \tag{3}$$

where

$$A_k = t_2 + t_5 e^{-ik_a} \tag{4}$$
$$B_k = 4t_4 e^{-i(k_a - k_b)/2} \cos(k_a/2) \cos(k_b/2) \tag{5}$$
$$C_k = 2e^{ik_b/2} \cos(k_b/2)(t_1 e^{-ik_a} + t_3) \tag{6}$$
$$D_k = 2e^{ik_b/2} \cos(k_b/2)(t_1 + t_3 e^{-ik_a}). \tag{7}$$

Here k_a=**k.a** and k_b=**k.b**, where **a**=a**x** and **b**=b**y** are the primitive translation vectors of phosphorene, see Fig. 1. The hopping integrals, t_i, have the following values: $t_1 = -1.220$ eV, $t_2 = 3.665$ eV, $t_3 = -0.205$ eV, $t_4 = -0.105$ eV, and $t_5 = -0.055$ eV[10]. From the tight-binding Hamiltonian (3) we can find the energy spectrum, $E_\alpha(\mathbf{k})$, and the corresponding wave functions, $\psi_\alpha(\mathbf{k})$. Here $\alpha = 1, 2, 3, 4$, where $\alpha = 1, 2$ correspond to two valence bands and $\alpha = 3, 4$ correspond to two conduction bands. The bandgap of phosphorene is ≈ 2 eV.

The electron dynamics in the external optical field is described by the time-dependent Schrödinger equation

$$i\hbar \frac{d\psi}{dt} = \mathcal{H}\psi \tag{8}$$

The applied optical pulse generates both interband and intraband electron dynamics. The interband electron dynamics causes redistribution of electrons between the valence and conduction bands, while the intraband electron dynamics determines the electron dynamics within a single band. Such intraband dynamics provides the main contribution to the charge transfer, which is studied below. The intraband electron dynamics is described by the universal acceleration theorem of the form

$$\hbar \frac{d\mathbf{k}}{dt} = \mathbf{F}(t), \tag{9}$$

which has the following solution

$$\mathbf{k}_T(\mathbf{q}, t) = \mathbf{q} + \frac{e}{\hbar} \int_{-\infty}^{t} \mathbf{F}(t_1) dt_1, \tag{10}$$

where $\mathbf{q}$ is the initial wave vector. Such intraband dynamics in the reciprocal space is incorporated into the corresponding wave functions through the Houston functions[34] of the form

$$\Phi_{\alpha q}^{(H)} = \psi_\alpha(\mathbf{k}_T(\mathbf{q}, t)) e^{-\frac{i}{\hbar}\int_{-\infty}^{t} dt_1 E_\alpha[\mathbf{k}_T(q, t_1)]}. \tag{11}$$

The Houston functions completely describe the intraband electron dynamics and are used below as a basis, so that the general solution of the time dependent Schrödinger equation (8) can be described as follows

$$\psi_q(t) = \sum_{\alpha=1,\ldots,4} \beta_{\alpha q}(t) \Phi_{\alpha q}^{(H)}. \tag{12}$$

The expansion coefficients $\beta_{\alpha q}(t)$ satisfy the following system of differential equations

$$\frac{d\beta_{\alpha q}}{dt} = -\frac{i}{\hbar} F_x \sum_{\alpha_1 \neq \alpha} Q_{\alpha\alpha_1}(t) \beta_{\alpha_1 q}, \tag{13}$$

where $\alpha, \alpha_1 = 1, \ldots, 4$. The time-dependent matrix $Q_{\alpha\alpha_1}(t)$ is determined by the x component of the dipole matrix elements between bands α and α_1

$$Q_{\alpha\alpha_1}(t) = D_{\alpha\alpha_1}^{(x)}[\mathbf{k}_T(\mathbf{q}, t)] \times e^{-\frac{i}{\hbar}\int_{-\infty}^{t} dt_1 [E_\alpha[\mathbf{k}_T(\mathbf{q}, t_1)] - E_{\alpha_1}[\mathbf{k}_T(\mathbf{q}, t_1)]]}, \tag{14}$$

where

$$D_{\alpha\alpha_1}^{(x)}(k) = < \psi_{\mathbf{k}}^{(\alpha)} | ex | \psi_{\mathbf{k}}^{(\alpha_1)} > = \hbar v_x^{\alpha\alpha_1} / i[E_{\alpha_1}(\mathbf{k}) - E_\alpha(\mathbf{k})]. \tag{15}$$

Here $v_x^{\alpha\alpha_1}$ are the matrix elements of the velocity operator, $v_x = \frac{1}{\hbar}\frac{\partial H_0}{\partial k_x}$.

The system of equations (13) describes the interband electron dynamics. We solve this system numerically

under the following initial conditions: $(\beta_1, \beta_2, \beta_3, \beta_4) = (1, 0, 0, 0)$ and $(\beta_1, \beta_2, \beta_3, \beta_4) = (0, 1, 0, 0)$, which correspond to initially occupied valence bands, i.e., bands 1 and 2. We characterize the interband dynamics, i.e., the solution of the system of equations (13), by the time-dependent conduction band populations $|\beta_{3,q}|^2$ and $|\beta_{4,q}|^2$. We also define the time-dependent total population of the conduction bands

$$\mathcal{N}_{CB,\alpha}(t) = \sum_{q,i} |\beta^{(i)}_{\alpha,q}(t)|^2, \tag{16}$$

where $\alpha = 3, 4$. The index $i = 1, 2$ corresponds to two initial conditions, which are described above.

The interband and intraband electron dynamics results not only in redistribution of electrons between the valence and conduction bands but also in generation of an electric current, which can be calculated from the following expression

$$J_x(t) = \frac{e}{ab} \sum_{i=1,2} \sum_{q} \sum_{\alpha_1,\alpha_2=1,\ldots,4} \beta^{(i)*}_{\alpha_1 q}(t) \upsilon_x^{\alpha_1\alpha_2} \beta^{(i)}_{\alpha_2 q}(t). \tag{17}$$

The generated current results in the charge transfer through the system, which is determined by

$$Q_{tr} = \int_{-\infty}^{\infty} dt J_x(t). \tag{18}$$

III. RESULTS AND DISCUSSION

The interband electron dynamics is characterized by electron redistribution between the valence and conduction bands and finally by finite conduction bands' populations. Such CBs populations are mainly determined by the strength of the interband dipole couplings, while the distribution of the CB population in the reciprocal space depends on the profile of the interband dipole matrix element in the reciprocal space. For example, in graphene, the interband dipole coupling is highly nonuniform in the reciprocal space and is singular at the Dirac points. Such singularities result in highly nonuniform electron distribution in the reciprocal space with hot spots near the Dirac points.

In phosphorene, which has a finite bandgap, ≈ 2 eV, the interband dipole matrix elements do not have any singularity in the reciprocal space. The interband dipole coupling is the strongest between the highest valence band and the lowest conduction band, i.e., between the bands 2 and 3. The corresponding dipole matrix element, D_{23}, is shown in Fig. 2 as a function of the reciprocal vector. The dipole matrix element D_{23} has a well pronounced maximum at the Γ point, $(0, 0)$. The other dipole matrix elements are almost constant within the whole Brillouin zone, see, for example, the dipole matrix element D_{12} shown in Fig. 2(a).

The maximum of the dipole matrix element D_{23} between the lowest CB and the highest VB results in specific distribution of the CB population in the reciprocal space. This is due to the fact that the strongest interband mixing occurs only when an electron, which is drifting through the reciprocal space according to the acceleration theorem, is near the Γ point, $(0, 0)$. In Fig. 3 the residual CB population, i.e., the electron CB population after the pulse, is shown for different amplitudes of the optical pulse. The data show that large CB population is localized near the Γ point. The hot spots near the Γ point are located symmetrically with respect to k_y-axis. The origin of such hot spots is the same as in graphene. They are due to interference, which happens when an electron passes twice through the Γ point during the pulse. The structure shown in Fig. 3 is similar to the one that was observed in graphene[33], but with one fundamental difference. In phosphorene, if an electron goes directly through the Γ point then the corresponding points of the hot spots have a maximum. In graphene, if an electron goes directly through the Dirac point then the corresponding intensity at the hot spots is zero. This is because the dipole matrix element has a singularity in graphene, but, but just a maximum in phosphorene.

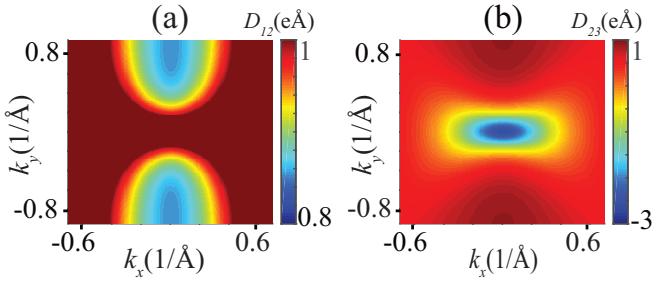

FIG. 2: Interband dipole matrix elements D_{12} and D_{23}. The dipole matrix elements are shown as functions of the wave vector **k**. Here D_{12} is the dipole matrix element between the valence bands 1 and 2, while D_{23} is the dipole matrix element between the highest valence band (band 2) and the lowest conduction band (band 3). The dipole matrix element $|D_{23}|$ has a maximum at the Γ point.

The time evolution of the CB population in the reciprocal space is shown in Fig. 4. The emergence of the hot spots as an electron passes through the region with large interband coupling is clearly visible. This behavior supports the above statement that the hot spots in the CB population distribution are due to electron passages through the region with large interband dipole matrix elements. The hot spots are localized due interference, which happens after two passages through the region with large interband coupling.

The number of hot spots in the CB population distribution increases with increasing field amplitude. This is because for a larger field amplitude, an electron travels a longer distance in the reciprocal space, see Eq. (9). The CB population of the first CB is shown in Fig. 3. The CB population of the second band is a few times smaller than the CB population of the first band (see discussion below). Its distribution in the reciprocal space also shows

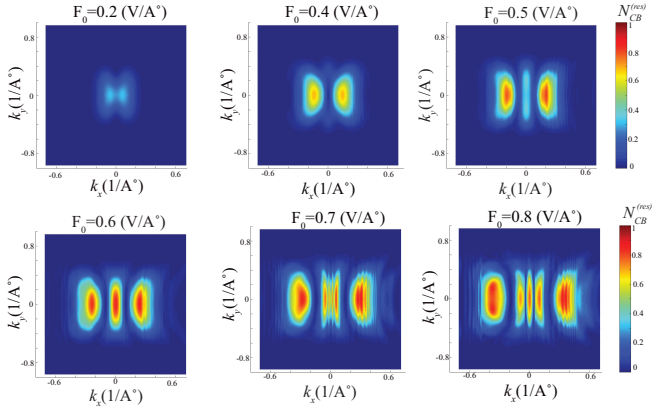

FIG. 3: Residual population of the first conduction band as a function of wave vector $\mathbf{k}$ for different amplitudes F_0 of the optical pulse, as indicated. The pulse is polarized along axis x.

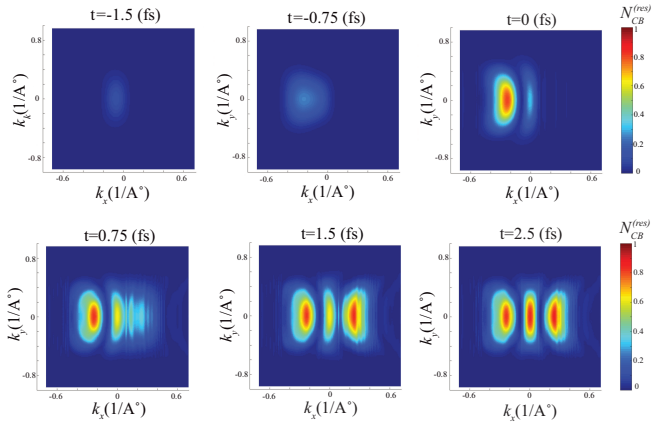

FIG. 4: Population of the first conduction band as a function of wave vector at different moments of time. The amplitude of the optical pulse is $F_0 = 0.6$ V/Å. Different colors correspond to different values of the conduction band population as shown in the figure.

the hot spots but they are much less pronounced.

The interband electron dynamics can be also characterized in terms of the time evolution of the total CB populations. The total CB populations of the first and the second CBs are shown in Fig. 5 for different amplitudes of the pulse. The data illustrate that the electron dynamics is highly irreversible, i.e., the maximum CB population during the pulse is comparable to the residual CB population after the pulse. This dynamics is similar to the one in gapless graphene. Although the phosphorene monolayer has a finite bandgap, $\Delta \approx 2$ eV, the gap is closed at the field amplitude $\approx \Delta/a \approx 0.4$ V/Å, where $a = 4.43$ Å.

The electron dynamics is highly irreversible, i.e., the system does not return to its initial state, which has zero CB populations, see Fig. 5. For $F_0 \lesssim 0.7$ eV/Å, the total

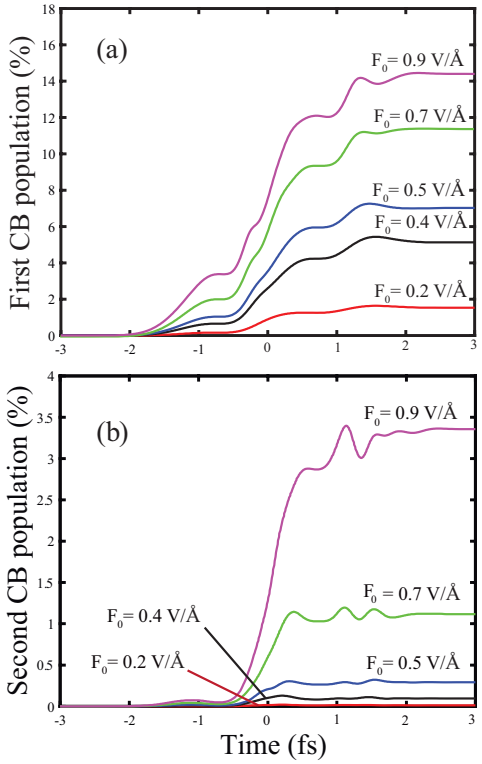

FIG. 5: (Conduction band population as a function of time. (a) Population of the first conduction band. (b) Population of the second conduction band. The peak fields are indicated on the graph.

population of the second CB is an order of magnitude smaller than the total population of the first CB, for example, at $F_0 = 0.7$ eV/Å, the residual CB population of the first band is 12 times lager than the residual CB population of the second band. At higher field amplitudes, the difference between the CB populations of the two bands becomes less pronounced. For example, at $F_0 = 0.9$ V/Å, the residual CB population of the first CB becomes only four times larger than the residual CB population of the second CB. The total residual CB populations for the first and second CBs, $N_1^{(res)}$ and $N_2^{(res)}$, respectively, are shown in Fig. 6 as the functions of the field amplitude. The residual CB population of the first band monotonically increases with field. Even at small field amplitudes, the residual CB population is relatively large. The residual CB population of the second band, $N_2^{(res)}$, is almost zero at $F_0 < 0.4$ V/Å and then it strongly increases with pulse intensity. This behavior is also illustrated in Fig. 6(b), where the ratio $N_1^{(res)}/N_2^{(res)}$ is shown. Here the transition from a large ratio, ~ 80, to a small ratio, ~ 5, occurs with increasing pulse amplitude.

Both interband and intraband electron dynamics generate an electric current through the system. Such current can be found from Eq. (17). The electric current has two contributions: interband current and intraband cur-

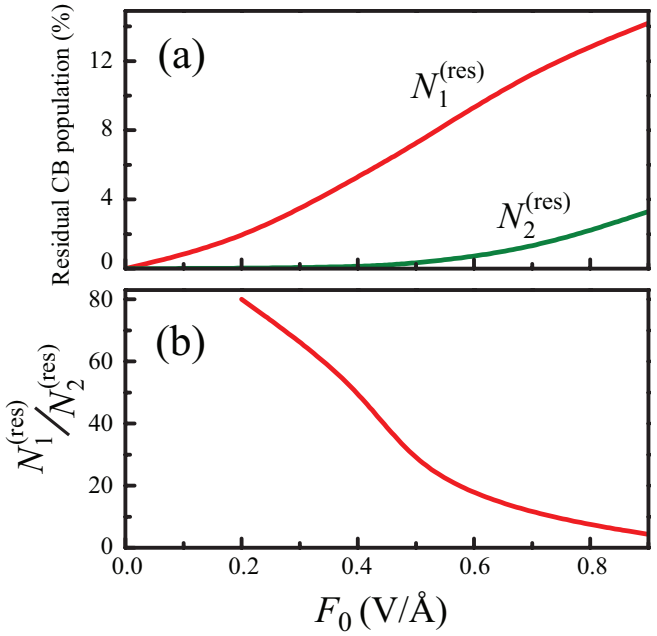

FIG. 6: (a) Residual conduction band population for the first, $N_1^{(res)}$), and the second, $N_1^{(res)}$), conduction bands as a function of the peak electric field, F_0. (b) Ratio of the residual conduction band populations, $N_1^{(res)})/N_2^{(res)}$).

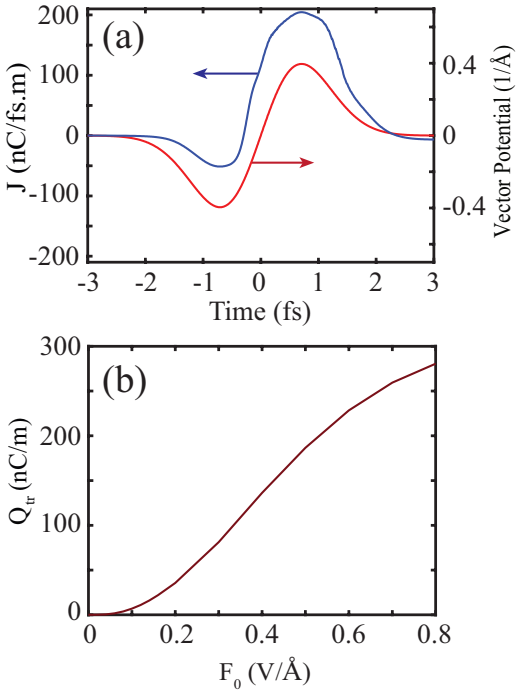

FIG. 7: (a) Electric current density and vector potential, $\int F(t)dt$, as a function of time. (b) Transferred charge density through phosphorene monolayer as a function of F_0.

rent. Usually, and also in our case of phosphorene, the main contribution to the electric current comes from the intraband term. The time dynamics of the electric current is shown in Fig. 7(a). The current follows the time integral of the electric field, i.e., the vector potential, $\int F(t)dt$. This behavior supports the above statement that the main contribution to the net electric current comes from the intraband term. The residual electric current is zero, which corresponds to residual electron population distribution that is symmetric with respect to k_y-axis. The area under the current vs time graph is the charge transferred through the system during the pulse, see Eq. (18). The transferred charge as a function of field amplitude is shown in Fig. 7(b). The transferred charge is positive for all field amplitudes. The positive sign of Q_tr means that the direction of the charge transfer is the same as the direction of the field maximum. This behavior is different from graphene, for which the transferred charge changes its sign from positive to negative with increasing pulse's intensity.

At small field amplitudes the transferred charge behaves as

$$Q_{tr} \propto F_0^3. \tag{19}$$

IV. CONCLUSION

The electron dynamics in a single layer of black phosphorus, i.e., phosphorene, in a strong field of an ultrashort optical pulse is highly irreversible, which means that the residual CB population is comparable to the maximum CB population during the pulse. Although the phosphorene has a relatively large bandgap, ≈ 2 eV, the irreversible electron dynamics in phosphorene is similar to the electron dynamics in other 2D materials, such as gappless graphene, silicene or germanene. The residual CB population in phosphorene is relatively large. It is about 20 % at the field amplitude $F_0 = 0.9$ V/Å. Here the population of the first CB is about 15 % while the population of the second CB band is 4 %. The distribution of the CB population in the reciprocal space shows hot spots that are located near the Γ point. These hot spots are due to two factors. The first one is that the interband dipole coupling has a maximum at the Γ point. Thus, during an electron field-induced transport in the reciprocal space the strongest interband coupling occurs when the electron passes the vicinity of the Γ point. The second factor, which determines the formation of the hot spots, is that the electron passes twice the Γ point. Such double passage results in formation of specific interference patterns in the CB population distribution. This behavior shows that, for a general system, by looking at the CB population distribution in the reciprocal space we can identify the positions of the maxima of the interband couplings in the system.

The electron dynamics in phosphorene is also characterized by the charge transfer through the system, which is proportional to the residual polarization of the phos-

phorene monolayer. The charge transfer through phosphorene occurs in the direction of the field maximum for all field amplitudes.

Acknowledgment

Major funding was provided by Grant No. DE-FG02-01ER15213 from the Chemical Sciences, Biosciences and Geosciences Division. Supplementary funding came from Grant No. DE-FG02-11ER46789 from the Materials Sciences and Engineering Division of the Office of the Basic Energy Sciences, Office of Science, U.S. Department of Energy, and Grant No. ECCS-1308473 from NSF.

[1] K. S. Novoselov, A. K. Geim, S. V. Morozov, D. Jiang, M. I. Katsnelson, I. V. Grigorieva, S. V. Dubonos, and A. A. Firsov, Nature **438**, 197 (2005).
[2] Y. B. Zhang, Y. W. Tan, H. L. Stormer, and P. Kim, Nature **438**, 201 (2005).
[3] A. K. Geim and K. S. Novoselov, Nat. Mater. **6**, 183 (2007).
[4] D. S. L. Abergel, V. Apalkov, J. Berashevich, K. Ziegler, and T. Chakraborty, Adv. Phys. **59**, 261 (2010).
[5] S. P. Koenig, R. A. Doganov, H. Schmidt, A. H. Castro Neto, and B. zyilmaz, Appl. Phys. Lett. **104**, 103106 (2014).
[6] C.-G. Andres, V. Leonardo, P. Elsa, O. I. Joshua, K. L. Narasimha-Acharya, I. B. Sofya, J. G. Dirk, B. Michele, A. S. Gary, J. V. Alvarez, et al., 2D Materials **1**, 025001 (2014).
[7] F. Xia, H. Wang, and Y. Jia, Nature Comm. **5**, 4458 (2014).
[8] H. Liu, A. T. Neal, Z. Zhu, Z. Luo, X. Xu, D. Tomnek, and P. D. Ye, ACS Nano **8**, 4033 (2014).
[9] L. Li, Y. Yu, G. J. Ye, Q. Ge, X. Ou, H. Wu, D. Feng, X. H. Chen, and Y. Zhang, Nat. Nano **9**, 372 (2014).
[10] E. Taghizadeh Sisakht, M. H. Zare, and F. Fazileh, Phys. Rev. B **91**, 085409 (2015).
[11] R. H. Fowler and L. Nordheim, Proc. Royal Soc. London. Ser. A **119**, 173 (1928).
[12] C. Zener, Proc. Royal Soc. A **145**, 523 (1934).
[13] L. V. Keldysh, J. Exptl. Theor. Phys. 33, 763-770 (1957); Translation: Sov. Phys. JETP **6**, 994 (1958).
[14] G. H. Wannier, Phys. Rev. **117**, 432 (1960).
[15] M. Lenzlinger and E. H. Snow, J. Appl. Phys. **40**, 278 (1969).
[16] M. Lenzner, J. Kruger, S. Sartania, Z. Cheng, C. Spielmann, G. Mourou, W. Kautek, and F. Krausz, Phys. Rev. Lett. **80**, 4076 (1998).
[17] L. Miaja-Avila, C. Lei, M. Aeschlimann, J. L. Gland, M. M. Murnane, H. C. Kapteyn, and G. Saathoff, Phys. Rev. Lett. **97**, 113604 (2006).
[18] M. I. Stockman, M. F. Kling, U. Kleineberg, and F. Krausz, Nat. Phot. **1**, 539 (2007).
[19] M. Durach, A. Rusina, M. F. Kling, and M. I. Stockman, Phys. Rev. Lett. **105**, 086803 (2010).
[20] M. Gertsvolf, M. Spanner, D. M. Rayner, and P. B. Corkum, J. Phys. B **43**, 131002 (2010).
[21] M. Durach, A. Rusina, M. F. Kling, and M. I. Stockman, Phys. Rev. Lett. **107**, 086602 (2011).
[22] S. Zherebtsov, T. Fennel, J. Plenge, E. Antonsson, I. Znakovskaya, A. Wirth, O. Herrwerth, F. Suessmann, C. Peltz, I. Ahmad, et al., Nat. Phys. **7**, 656 (2011).
[23] M. Kruger, M. Schenk, and P. Hommelhoff, Nature **475**, 78 (2011).
[24] S. Ghimire, A. D. DiChiara, E. Sistrunk, P. Agostini, L. F. DiMauro, and D. A. Reis, Nature Phys. **7**, 138 (2011).
[25] A. Schiffrin, T. Paasch-Colberg, N. Karpowicz, V. Apalkov, D. Gerster, S. Muhlbrandt, M. Korbman, J. Reichert, M. Schultze, S. Holzner, et al., Nature **493**, 70 (2012).
[26] M. Schultze, E. M. Bothschafter, A. Sommer, S. Holzner, W. Schweinberger, M. Fiess, M. Hofstetter, R. Kienberger, V. Apalkov, V. S. Yakovlev, et al., Nature **493**, 75 (2013).
[27] F. Krausz and M. I. Stockman, Nat Photon **8**, 205 (2014).
[28] A. V. Mitrofanov, A. J. Verhoef, E. E. Serebryannikov, J. Lumeau, L. Glebov, A. M. Zheltikov, and A. Baltuška, Phys. Rev. Lett. **106**, 147401 (2011).
[29] V. Apalkov and M. I. Stockman, Phys. Rev. B **88**, 245438 (2013).
[30] H. K. Kelardeh, V. Apalkov, and M. I. Stockman, Phys. Rev. B **90**, 085313 (2014).
[31] H. K. Kelardeh, V. Apalkov, and M. I. Stockman, Phys. Rev. B **92**, 045413 (2015).
[32] H. K. Kelardeh, V. Apalkov, and M. I. Stockman, Phys. Rev. B **93**, 155434 (2016).
[33] H. K. Kelardeh, V. Apalkov, and M. I. Stockman, Phys. Rev. B **91**, 0454391 (2015).
[34] W. V. Houston, Phys. Rev. **57**, 184 (1940).